

Three-Dimensional Nonlinear Lattices: From Oblique Vortices and Octupoles to Discrete Diamonds and Vortex Cubes

R. Carretero-González,¹ P. G. Kevrekidis,² B. A. Malomed,³ and D. J. Frantzeskakis⁴

¹*Nonlinear Dynamical Systems Group, Department of Mathematics and Statistics, San Diego State University, San Diego California 92182-7720, USA*

²*Department of Mathematics and Statistics, University of Massachusetts, Amherst, Massachusetts 01003-4515, USA*

³*Department of Interdisciplinary Studies, Faculty of Engineering, Tel Aviv University, Tel Aviv 69978, Israel*

⁴*Department of Physics, University of Athens, Panepistimiopolis, Zografos, Athens 15784, Greece*

(Received 11 January 2005; published 23 May 2005)

We construct a variety of novel localized topological structures in the 3D discrete nonlinear Schrödinger equation. The states can be created in Bose-Einstein condensates trapped in strong optical lattices and crystals built of microresonators. These new structures, most of which have no counterparts in lower dimensions, range from multipole patterns and diagonal vortices to vortex “cubes” (stack of two quasiplanar vortices) and “diamonds” (formed by two orthogonal vortices).

DOI: 10.1103/PhysRevLett.94.203901

PACS numbers: 42.65.Tg, 03.75.Lm

Introduction.—Recently, much attention has been paid to the study of intrinsic localized modes (ILMs, *alias* discrete solitons) in nonlinear dynamical lattices, especially due to the ability of such modes to act as energy “hot spots” [1]. The relevance of ILMs has been demonstrated in problems ranging from arrays of nonlinear-optical waveguides [2] and photonic crystals [3] to Bose-Einstein condensates (BECs) trapped in optical lattices (OLs) [4,5] and Josephson-junction ladders [6].

A universal model, which may arise as an envelope approximation from most of the complex nonlinear equations on the lattice and also as a direct physical model for BECs [4] and optical waveguide arrays [7], is the discrete nonlinear Schrödinger (DNLS) equation [8]. On top of its significance to applications, the DNLS equation itself is a fundamentally interesting dynamical model. In the 3D case, its direct physical realization is provided, as mentioned above, by BECs trapped in strong OLs [4]. Waveguide arrays, however, cannot be described by a 3D discrete model, since the evolution variable in the optical media is a spatial coordinate, while the temporal variable, which effectively plays the role of an additional quasi-spatial one, cannot be discrete. Nevertheless, another physical realization of the 3D DNLS equation may be provided by a crystal built of microresonators [9].

The study of the 3D continuum NLS equation, including a 3D [10] or quasi-2D [11] OL, and of the DNLS model proper [12] has started recently, becoming accessible to numerical computations. As a result, the first coherent structures, such as discrete vortices of the topological charge (vorticity) $S = 1, 2$, and 3, were identified and their stability was investigated. The aim of the present work is to study a large variety of novel localized 3D structures in the DNLS equation, many of which turn out to be stable. In particular, we first construct states which include dipoles with the axis oriented along a lattice bond, or along a planar diagonal, or along a 3D diagonal (we call them,

respectively, “straight,” “oblique,” and “diagonal” dipoles). Next, we construct quadrupole and octupole states, that, similar to the dipoles, are real solutions. More complex structures are also found, namely, “vortex cubes” (a stack of two straight vortices with the same or opposite charges centered on parallel planes), oblique and diagonal vortices, and “vortex diamonds,” formed by a crossed pair of vortices with orthogonal axes. Apart from the quadrupoles and straight and oblique dipoles, these ILMs have no counterparts in 2D lattices.

To present the results, we first introduce the model, and then report systematic results for the shape and stability of the new localized states. This is followed by conclusions, including an explanation for the stability and instability of the majority of patterns found in this work.

The model.—We consider the DNLS equation on the cubic lattice with a coupling constant C [12],

$$i\dot{\phi}_{l,m,n} + C\Delta\phi_{l,m,n} + |\phi_{l,m,n}|^2\phi_{l,m,n} = 0, \quad (1)$$

where $\dot{\phi} = d\phi/dt$, and the discrete Laplacian is $\Delta\phi_{l,m,n} \equiv \phi_{l+1,m,n} + \phi_{l,m+1,n} + \phi_{l,m,n+1} + \phi_{l-1,m,n} + \phi_{l,m-1,n} + \phi_{l,m,n-1} - 6\phi_{l,m,n}$. Solutions are looked for as $\phi_{l,m,n} = u_{l,m,n} \exp(i\Lambda t)$ with a frequency $-\Lambda$ (or the chemical potential in the context of BECs), where the stationary functions $u_{l,m,n}$ obey the equation

$$\Lambda u_{l,m,n} = C\Delta u_{l,m,n} + |u_{l,m,n}|^2 u_{l,m,n}. \quad (2)$$

Profiles used as an initial guess for the fixed-point iteration converging to solutions displayed below were based on the form of the respective solutions (for the same Λ) in the anticontinuum (AC) limit, $C = 0$. Once solutions to Eq. (2) have been obtained, the linear-stability analysis is performed for a perturbed solution [12], $\phi_{l,m,n} = [u_{l,m,n} + \epsilon(a_{l,m,n}e^{\lambda t} + b_{l,m,n}e^{\lambda^* t})]e^{i\Lambda t}$, where ϵ is an infinitesimal amplitude of the perturbation, and λ is its eigenvalue. The Hamiltonian nature of the system dictates that if λ is

an eigenvalue, then so are $-\lambda$, λ^* , and $-\lambda^*$ (in the stable case, λ is imaginary; hence this symmetry yields only two different eigenvalues, λ and $-\lambda$). The stationary solution is unstable if at least one pair of the eigenvalues features nonvanishing real parts.

Results.—We start by constructing purely real solutions of the dipole type (in lower-dimensional models, solitons of this type were considered in Refs. [13,14]). Figure 1 displays examples of “tight” dipoles with adjacent excited sites (i.e., the separation between them is $d = 1$, in the corresponding units) and three possible orientations relative to the lattice: (a) *straight* (along a lattice’s bond), (b) *oblique* (along a planar diagonal), and (c) *diagonal* (along a 3D diagonal). In this figure and in the text that follows, unless stated otherwise, we show a typical case admitting stable solutions, with $C = 0.1$ and $\Lambda = 2$. The borders of the stability windows, $0 \leq C \leq C_{\text{dip}}^{(3D,d)}$, for the three types (straight, oblique, and diagonal) of the dipoles are given by $C_{\text{dip-str}}^{(3D,1)} = 0.23013 \pm \delta C$, $C_{\text{dip-obl}}^{(3D,1)} = 0.53666 \pm \delta C$, and $C_{\text{dip-dia}}^{(3D,1)} = 0.73084 \pm \delta C$, where the error margin is $\delta C = 0.00001$. We observe that the diagonal dipole in Fig. 1(c) remains stable in a larger interval than its oblique counterparts in Fig. 1(b), which, in turn, is more stable than the straight one in Fig. 1(a). It is also possible to construct dipole solutions corresponding to $d = 2$, with excited sites separated by a single nearly empty site. Such dipole solutions (not depicted here) have larger stability windows than their tight ($d = 1$) counterparts: $C_{\text{dip-str}}^{(3D,2)} = 0.66722$, $C_{\text{dip-obl}}^{(3D,2)} = 1.08024$, and $C_{\text{dip-dia}}^{(3D,2)} = 1.31356$. As seen in Fig. 1(h), $C_{\text{dip}}^{(3D,d)}$ further increases with the separation distance d , approaching the stability threshold of the fundamental (single-site-based) discrete soliton, $C_{\text{dip}}^{(3D,\infty)} \equiv C_{\text{fund}}^{(3D)} = 2.009 \pm 0.001$ [12]; see the horizontal dashed line in the figure. It can also be found that the same relations, $0 < C_{\text{dip-str}}^{(3D,d)} < C_{\text{dip-obl}}^{(3D,d)} < C_{\text{dip-dia}}^{(3D,d)}$, as found for $d = 1$ are valid for all d ; see Fig. 1(h). Another relevant comparison is with dipoles in the 2D DNLS model, which were studied in Ref. [15]. The comparison shows that oblique and straight dipole solitons, which have their counterparts in the 2D case, are less stable, although not drastically, than those counterparts: $C_{\text{dip-str}}^{(3D,1)} = 0.23013 < C_{\text{dip-str}}^{(2D,1)} = 0.245 \pm 0.005$ for $\Lambda = 2$. The weaker stability of the 3D structures is explained by the analogy with the continuum NLS equation, where solitons are destabilized by collapse, which is, respectively, *weak* and *strong* in the 2D and 3D cases [16].

Quadrupole and octupole solitons are also shown in Fig. 1. The quadrupole is based on four contiguous sites ($d = 1$) which form a square in the plane, Fig. 1(d). It is found to be stable for $C < C_{\text{quad}}^{(3D,1)} = 0.13836$, while its 2D analog has $C_{\text{quad}}^{(2D,1)} = 0.1485 \pm 0.0005$ [17]. Again, as for the dipoles, the 2D configurations tend to be slightly more

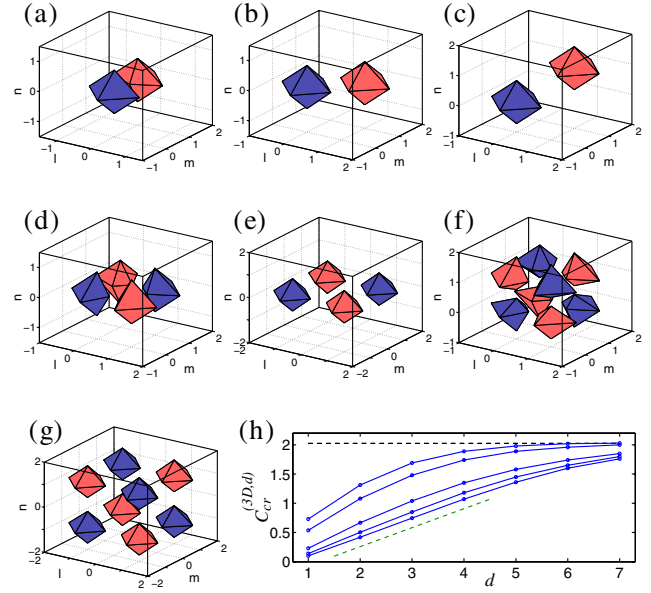


FIG. 1 (color online). Stable multipoles. The top row depicts stable tight dipoles ($d = 1$): (a) straight, (b) oblique, and (c) diagonal ones. (d),(e) Quadrupoles in the $n = 0$ plane, with internal separation $d = 1$ and $d = 2$, respectively. (f),(g) Octupoles with $d = 1$ and $d = 2$. Panel (h) displays the stability threshold $C_{\text{cr}}^{(3D,d)}$ as a function of the internal distance d for (from top to bottom) diagonal, oblique, and straight dipoles, octupoles, and quadrupoles. The horizontal dashed line corresponds to the stability threshold for the fundamental discrete soliton. Note that, for the quadrupole (bottom graph), $C_{\text{quad}}^{(3D,d)}$ behaves linearly for small d (see the dashed line with slope 0.325 for guidance). In panels (a)–(g), level contour corresponding to $\text{Re}(u_{l,m,n}) = \pm 0.5$ are shown in blue (dark gray) and red (gray), respectively. All these states are *stable* (for the case shown, with $\Lambda = 2$ and $C = 0.1$).

stable than their 3D siblings. The octupole is shown in Fig. 1(f); it is based on a set of eight contiguous sites ($d = 1$ as well) forming a cubic cell in the 3D lattice. It is stable in the interval $C < C_{\text{oct}}^{(3D,1)} = 0.10030$, which is smaller than the above ones for the quadrupoles and dipoles. Similar to the dipoles, multipoles can also “swell” by inserting unpopulated sites between the excited ones. The resulting stability intervals for $d = 2$ are larger than their $d = 1$ counterparts: $C_{\text{quad}}^{(3D,2)} = 0.503232$ and $C_{\text{oct}}^{(3D,2)} = 0.418411$; see Figs. 1(e) and 1(g), respectively. It is relevant to mention that all the newly found structures have their stability limits lower than the above-mentioned limit for the fundamental (single-site-based) discrete soliton, $C_{\text{fund}}^{(3D)} = 2.009 \pm 0.001$ [12]; see Fig. 1(h).

Stable dipoles have one pair of imaginary eigenvalues in their stability spectrum that, with the increase of C , collides with the continuous spectrum, which leads to the destabilization. On the other hand, stable quadrupoles have three such pairs (two of them form a doublet for small C), and the octupoles have seven (six of which

form two triplets for small C). More generally, the number of potentially unstable eigenvalue pairs is $N - 1$, where N is the number of sites on which the structure is based [18].

The next novel type of a 3D discrete soliton, with no lower-dimensional counterpart, is a vortex cube, which is built as a stack of two quasiplanar vortices with equal topological charges $S_1 = S_2 = 1$ and a phase shift $\Delta\phi = \pi$, separated by an empty layer, so that it has $d = 2$. Figure 2(a) shows real and imaginary parts of the vortex-cube lattice field. Such a state is stable for $0 \leq C \leq C_{\text{cub},\pi}^{(3D,2)} = 0.56324$. On the contrary, a vortex cube built as a stack of two in-phase vortices ($\Delta\phi = 0$) is *always unstable*, through three real eigenvalue pairs. Further, Fig. 2(b) shows a similar stack, but composed of two vortices with opposite charges, $S_1 = -S_2 = 1$. This configuration is *always unstable* as well, due to a real eigenvalue pair. The instability is manifested as a symmetry breaking between the two planes leading to the loss of phase coherence of the pattern; see Fig. 2(c).

Another 3D object, with no lower-dimensional analog either, is a vortex with the axis directed along the diagonal of the cubic lattice, i.e., the vector $(1, 1, 1)$. Figure 3(a) shows such a “diagonal vortex” constructed by a continuation procedure starting, in the AC limit, with the following distribution of phases: $\phi_{l,m,n} = 2\pi S k / 6$ ($k = 0, 1, 2, \dots, 5$) for the sites that lie in a plane orthogonal to the axial (diagonal) direction: $(1, -1, 0)$, $(0, -1, 1)$, $(-1, 0, 1)$, $(-1, 1, 0)$, $(0, 1, -1)$, $(1, 0, -1)$. Obviously, this phase pattern bears the vorticity S ($S = 1$ in Fig. 3). However, the diagonal vortex turns out to be *always unstable*, due to three real eigenvalue pairs, and it eventually settles to a single-site-based soliton.

One more species of discrete vortices that may exist solely in the 3D lattice is an oblique one, shown in Figs. 3(b) and 3(c), with the axis directed along $(1, 1, 0)$. In the AC limit, the solution is carried by the array of sites $(1, -1, 0)$, $(1, -1, 1)$, $(0, 0, 1)$, $(-1, 1, 1)$, $(-1, 1, 0)$, $(-1, 1, -1)$, $(0, 0, -1)$, and $(1, -1, -1)$, with respective phases $S \cdot (0, \alpha, \pi/2, \alpha + \pi/2, \pi, \alpha + \pi, 3\pi/2, \alpha + 3\pi/2)$,

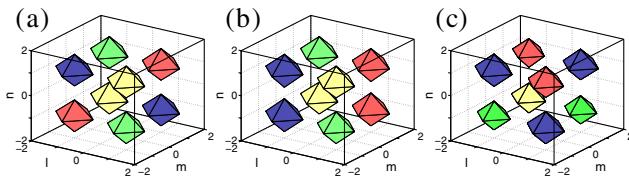


FIG. 2 (color online). Vortex cubes for $\Lambda = 2$ and $C = 0.1$. Panel (a) shows a *stable* vortex cube, built of two quasiplanar vortices with equal vorticities, $S_1 = S_2 = 1$, and a phase shift of π . Panel (b) shows an unstable cube formed by vortices with opposite charges, $S_1 = -S_2$, and panel (c) shows a snapshot (at $t = 200$) of its evolution, clearly demonstrating that the phase coherence is lost. The real level contours are as in Fig. 1, and the imaginary ones, $\text{Im}(u_{l,m,n}) = \pm 0.5$, are shown by green (light gray) and yellow (very light gray) hues, respectively.

where $\alpha \equiv \tan^{-1}(1/\sqrt{2})$. Figure 3(b) depicts such an oblique vortex, which, in this form, is found to be *always unstable*, similar to the diagonal vortex. Nonetheless, the oblique vortex can be stabilized in a modified form, by introducing a sign shift at the intermediate edge sites [i.e., $(0, 0, 1)$, $(-1, 1, 0)$, $(0, 0, -1)$, and $(1, -1, 0)$]; see Fig. 3(c). This sign change avoids having contiguous sites with the same phase and does not alter the vortex’s topological charge, which remains 1. The modified oblique vortex is stable in a small interval, $C < C_{\text{vor-obl}}^{(3D)} = 0.0104$.

Finally, motivated by the concept of Skyrmions [19], which are distinguished by two topological charges associated with closed contours in two perpendicular planes, we have constructed one more type of vortex structures in the 3D lattice, viz., a “diamond” shown in Fig. 4(a). It is built as a vortex cross, i.e., a nonlinear superposition of two straight $S = 1$ vortices, with axes directed along two orthogonal directions. The stability analysis shows that it is *always unstable* due to a real eigenvalue pair. The instability manifests itself in a rather intriguing manner; see Fig. 4(b). At $t \approx 100$, two pairs of opposite vertices change phases (one by $+\pi$ and the other by $-\pi$). After this, the diamond remains stable until $t \approx 200$, when the same pairs of sites suffer a second phase shift (in the same direction) and the configuration returns to its original phase distribution. This process repeats itself almost periodically [together with small amplitude variations of $\pm 10\%$; see the top panel of Fig. 4(b)] until the phase coherence is finally lost and the solution degenerates into a plain single-site-based soliton.

Conclusions and discussion.—We have introduced several novel species of topologically structured discrete solitons in 3D dynamical lattices, using the paradigm of the discrete nonlinear Schrödinger equation. The solutions have been constructed starting from properly chosen anti-continuum approximations, and their linear stability has been studied. Previously, only the fundamental single-site-based solitons and straight vortices, with the axis directed along a lattice bond, were known. We have found three species of dipoles which differ by the orientation relative to the lattice, quadrupoles and octupoles, vortex cubes (stacked dual-vortex patterns), diagonal and oblique vorti-

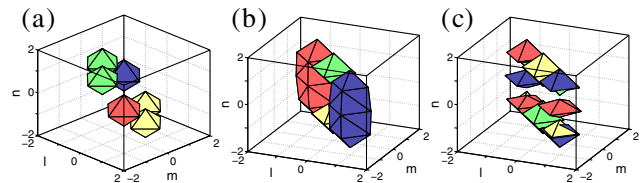


FIG. 3 (color online). Diagonal and oblique vortices. Panel (a) shows an unstable diagonal vortex, with the axis along the direction $(1, 1, 1)$, for $\Lambda = 2$ and $C = 0.1$. Panel (b) shows an unstable oblique vortex with the axis oriented along the direction $(1, 1, 0)$, and panel (c) shows a *stable* oblique vortex of a modified form (see text) for $\Lambda = 2$ and $C = 0.01$.

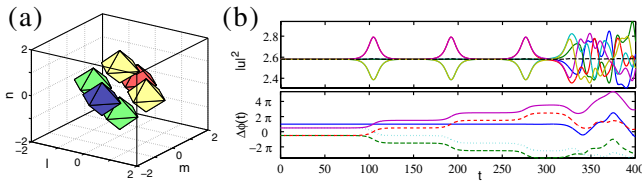


FIG. 4 (color online). The vortex diamond for $\Lambda = 2$ and $C = 0.1$. Panel (a) displays an unstable diamond, and panel (b) depicts its evolution, in terms of the field's magnitude (top) and phase (bottom) at the main six lattice sites. Initially ($t < 300$), pairs of sites (opposite vertices of the diamond) cyclically change the phase, and subsequently ($t > 350$) the phase coherence is lost and the field magnitude oscillates erratically about its initial level.

ces, and diamonds (vortex crosses or discrete Skyrmions). Except for the straight and oblique dipoles and quadrupoles, the patterns obtained are endemic to the 3D lattice setting, having no counterparts in lower dimensions.

Apart from the diagonal vortices and diamonds, all the patterns constructed above have stability regions below a critical value of the coupling parameter. It is possible to explain the stability or instability of all the structures realized as bound states of simpler objects, viz., dipoles, quadrupoles (bound states of two dipoles with opposite orientations), octupoles (bound states of two quadrupoles), and vortex cubes. Indeed, a known general principle is that a bound state pinned by the lattice may be stable only if the coupled objects *repel* each other [15,20] (i.e., have a phase difference of π between their building blocks). This explains the existence of stability regions for multipoles of all types. Similarly, considering the interaction between constituent quasiplanar vortices, one may understand the stability and instability of vortex cubes of the types shown in Figs. 2(a) and 2(b), respectively. Following this principle, it is also possible to predict the stability of more exotic 3D patterns, such as bound states of two oblique or diagonal dipoles, or octupoles constructed of two such states. In those cases when the 3D structures have 2D counterparts, viz., straight and oblique dipoles and quadrupoles, their stability regions are narrower than in the 2D case, which is explained by a stronger trend to collapse in three dimensions. Future challenges involve semianalytical investigation of such solutions via the Lyapunov-Schmidt theory, and identification of their stability by means of methods similar to those developed for the 1D and 2D cases [18].

The findings presented in this manuscript may pave the way for the observation of stable bound state configurations of solitary waves and vortices such as the ones identified herein. This is in sharp contrast to the continuum

case, where such configurations would be strongly unstable towards collapse. The experimental realization of 3D optical lattices in Bose-Einstein condensates may provide the most fertile ground for the observation of lattice-induced stabilization of such configurations [5].

-
- [1] S. Aubry, *Physica* (Amsterdam) **103D**, 201 (1997); S. Flach and C.R. Willis, *Phys. Rep.* **295**, 181 (1998); D.N. Christodoulides *et al.*, *Nature* (London) **424**, 817 (2003); D.K. Campbell *et al.*, *Phys. Today* **57**, No. 1, 43 (2004).
 - [2] See, e.g., A.A. Sukhorukov, Y.S. Kivshar, H.S. Eisenberg, and Y. Silberberg, *IEEE J. Quantum Electron.* **39**, 31 (2003); U. Peschel *et al.*, *J. Opt. Soc. Am. B* **19**, 2637 (2002).
 - [3] S.F. Mingaleev and Y.S. Kivshar, *Phys. Rev. Lett.* **86**, 5474 (2001).
 - [4] A. Trombettoni and A. Smerzi, *Phys. Rev. Lett.* **86**, 2353 (2001); F.Kh. Abdullaev *et al.*, *Phys. Rev. A* **64**, 043606 (2001); F.S. Cataliotti *et al.*, *Science* **293**, 843 (2001); A. Smerzi *et al.*, *Phys. Rev. Lett.* **89**, 170402 (2002); G.L. Alfimov *et al.*, *Phys. Rev. E* **66**, 046608 (2002); R. Carretero-González and K. Promislow, *Phys. Rev. A* **66**, 033610 (2002).
 - [5] M. Greiner *et al.*, *Nature* (London) **415**, 39 (2002).
 - [6] P. Binder *et al.*, *Phys. Rev. Lett.* **84**, 745 (2000); E. Trías *et al.*, *Phys. Rev. Lett.* **84**, 741 (2000).
 - [7] D.N. Christodoulides and R.I. Joseph, *Opt. Lett.* **13**, 794 (1988); A. Aceves *et al.*, *Opt. Lett.* **19**, 1186 (1994); H.S. Eisenberg *et al.*, *J. Opt. Soc. Am. B* **19**, 2938 (2002); J. Meier *et al.*, *Phys. Rev. Lett.* **91**, 143907 (2003).
 - [8] P.G. Kevrekidis, K. Ø. Rasmussen, and A.R. Bishop, *Int. J. Mod. Phys. B* **15**, 2833 (2001).
 - [9] J.E. Heebner and R.W. Boyd, *J. Mod. Opt.* **49**, 2629 (2002); P. Chak *et al.*, *Opt. Lett.* **28**, 1966 (2003).
 - [10] B.B. Baizakov *et al.*, *J. Phys. B* **35**, 5105 (2002); B.B. Baizakov *et al.*, *Europhys. Lett.* **63**, 642 (2003).
 - [11] B.B. Baizakov *et al.*, *Phys. Rev. A* **70**, 053613 (2004).
 - [12] P.G. Kevrekidis, B. Malomed, D.J. Frantzeskakis, and R. Carretero-González, *Phys. Rev. Lett.* **93**, 080403 (2004).
 - [13] P.G. Kevrekidis *et al.*, *Phys. Rev. E* **65**, 016605 (2002).
 - [14] J. Yang *et al.*, *Opt. Lett.* **29**, 1662 (2004).
 - [15] P.G. Kevrekidis *et al.*, *J. Phys. A* **34**, 9615 (2001).
 - [16] C. Sulem and P.L. Sulem, *The Nonlinear Schrödinger Equation* (Springer-Verlag, New York, 1999).
 - [17] P.G. Kevrekidis *et al.*, *Phys. Rev. E* **70**, 056612 (2004).
 - [18] D.E. Pelinovsky, P.G. Kevrekidis, and D.J. Frantzeskakis, *nlin.PS/0411016*; *nlin.PS/0410005*.
 - [19] T.H.R. Skyrme, *Proc. R. Soc. A* **260**, 127 (1961).
 - [20] T. Kapitula *et al.*, *Phys. Rev. E* **63**, 036604 (2001).